Supplementary Information for

Self-templated induced carbon supported hollow WS_2 composite structure for high performance sodium storage

Xiaomin Luo[a], Jianfeng Huang[a,], Yixuan Huang[b], Liyun Cao[a], *, Jiayin Li[a,*], Yuhang Wang[a], Zhanwei Xu[a], Shiying Wei[a], Koji Kajiyoshi[c]*

a School of Material Science and Engineering, International S&T Cooperation Foundation of Shaanxi Province, Xi'an Key Laboratory of Green Manufacture of Ceramic Materials, Shaanxi University of Science and Technology, Xi'an 710021, China

b Department of Chemical Engineering, Monash University, Clayton, Victoria 3168, Australia

c Kochi University, Research Laboratory of Hydrothermal Chemistry, Kochi 780-8520, Japan

E-mail: huangjf@sust.edu.cn

caoliyun@sust.edu.cn

lijiayin@sust.edu.cn

Supporting Information

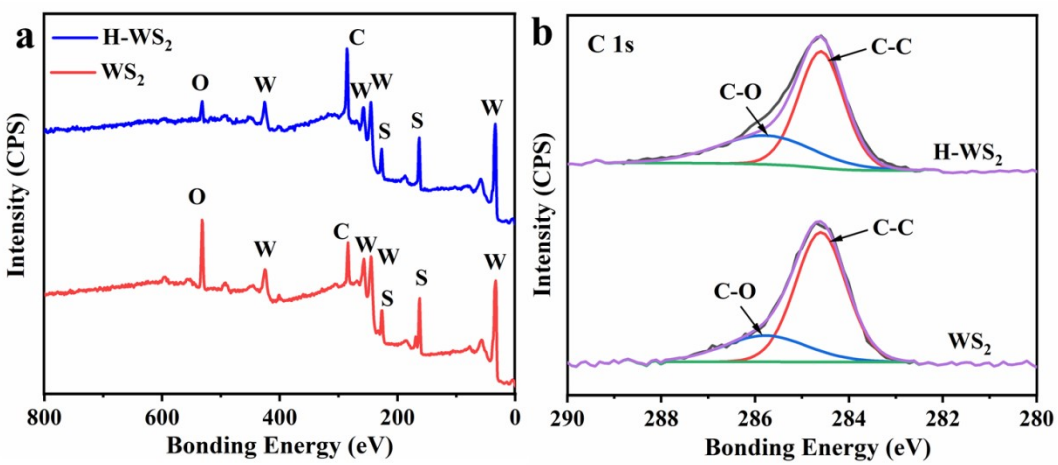

Fig. S1 XPS full survey spectra of H-WS_2 and WS_2 (a), high-resolution XPS spectra of H-WS_2 and WS_2 for C 1s.

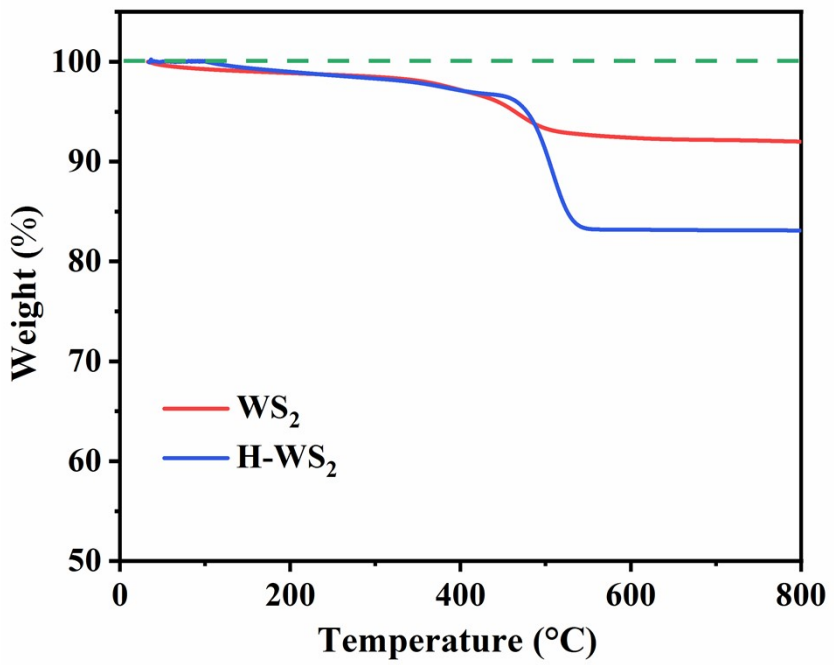

Fig. S2. TGA curves of WS_2, and H-WS_2.

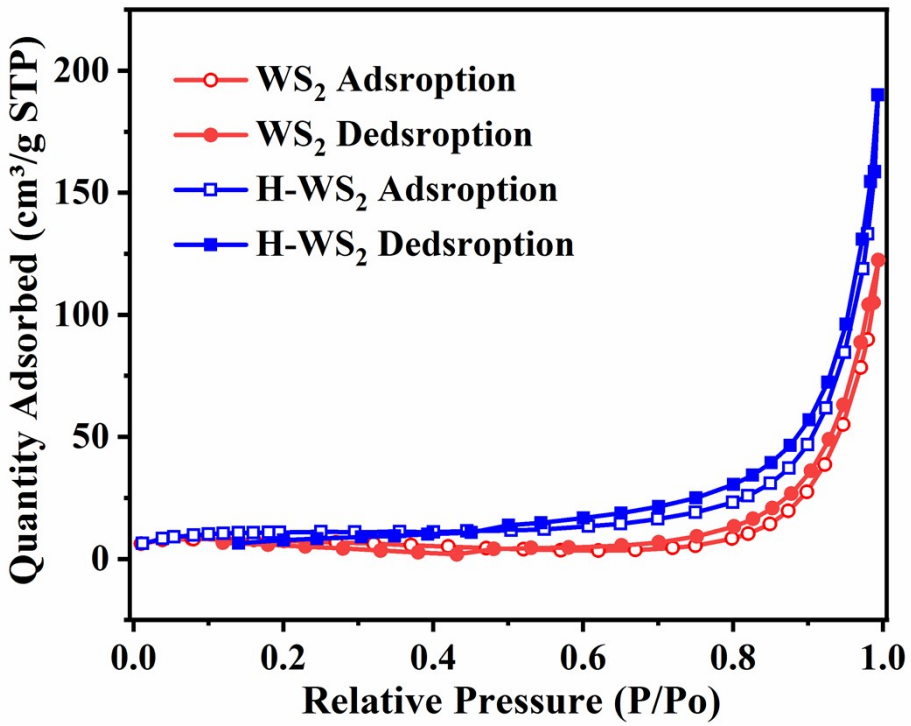

Fig. S3. N_2 adsorption–desorption isotherms of the WS_2, and H-WS_2.

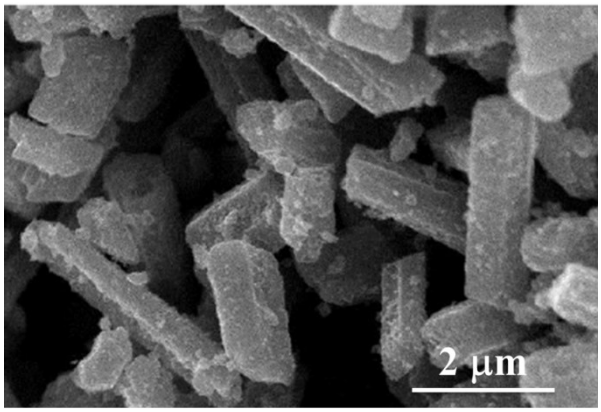

Fig. S4 The morphology of glucose.

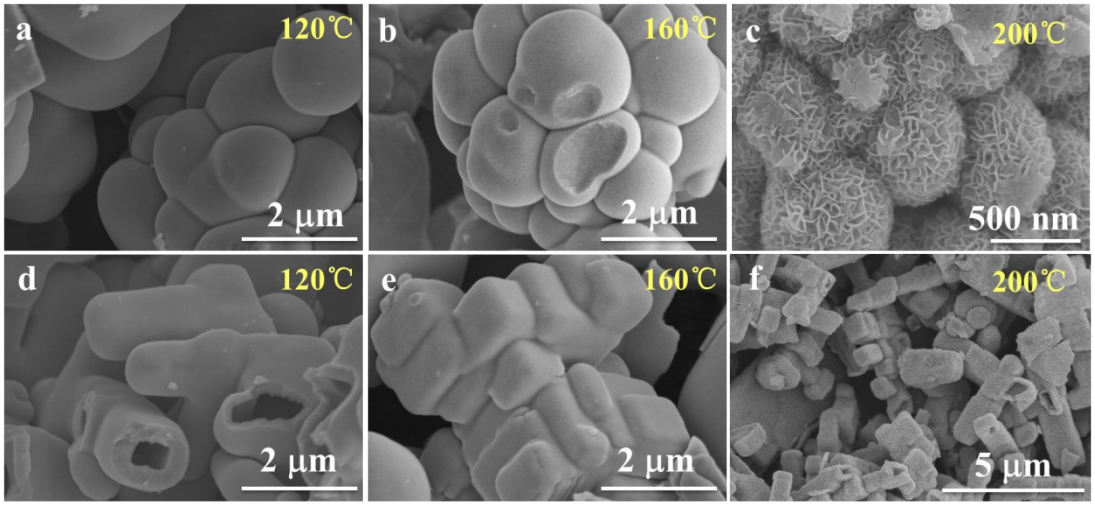

Fig. S5 The SEM images of WS_2 at 120 °C(a); 160 °C (b); 200 °C (c) for 24h, the SEM images of H-WS_2 at 120 °C (d); 160 °C (e); 200 °C (f) for 24 h.

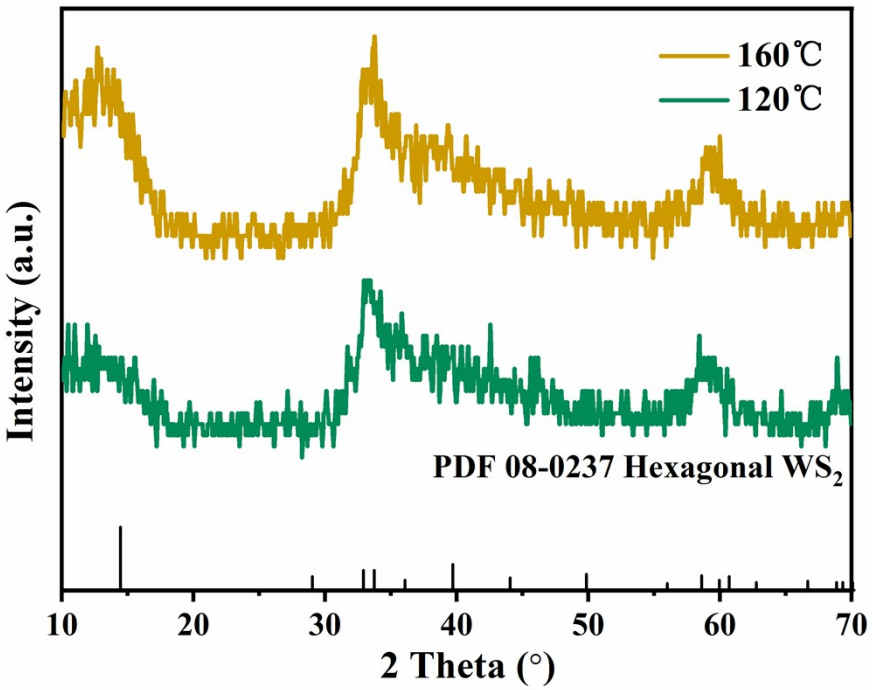

Fig. S6 The XRD patterns of WS_2 at 120 °C and 160 °C for 24h.

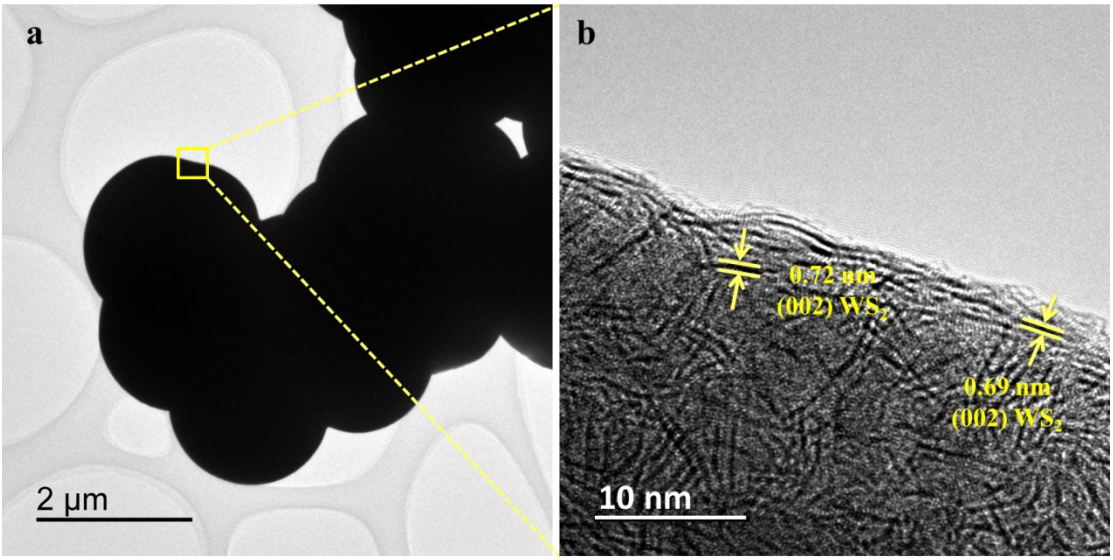

Fig. S7 The TEM image (a) and HRTEM image (b) of WS_2 at 120 °C for 24h.

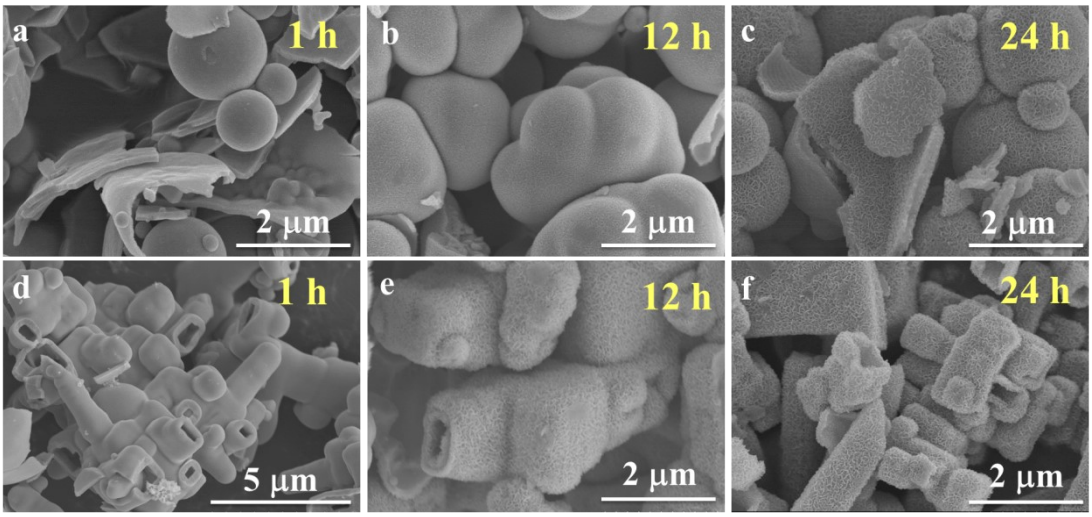

Fig. S8 The SEM images of WS_2 at 200 °C for 1 h (a); 12 h (b) and 24 h (c), the SEM images of H-WS_2 at 200 °C for 1 h (d); 12 h (e) and 24 h (f).

Fig. S9 The pictures of glucose solvothermal in ethanol at 120 °C (a); 160 °C (b); 200 °C (c) for 24 h.

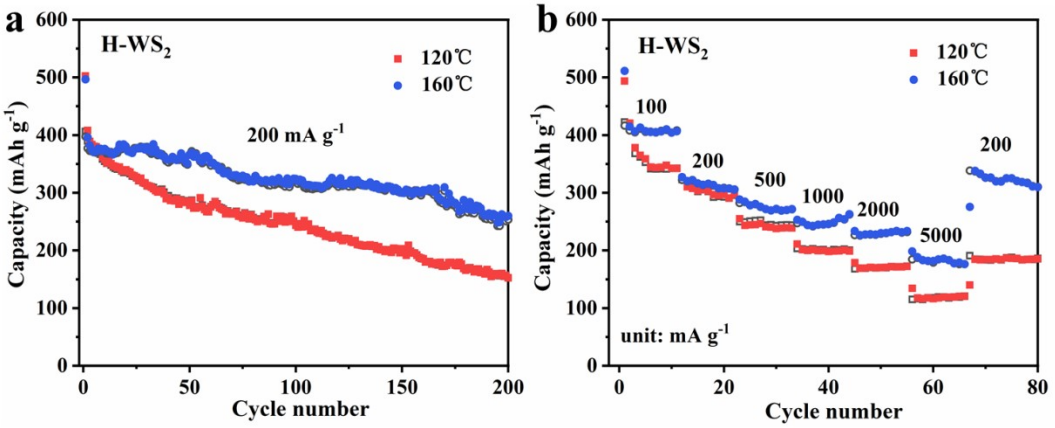

Fig. S10. Electrochemical performance of H-WS_2 electrodes at 120 °C and 160 °C; (a) cycle performance; (b) rate capability.

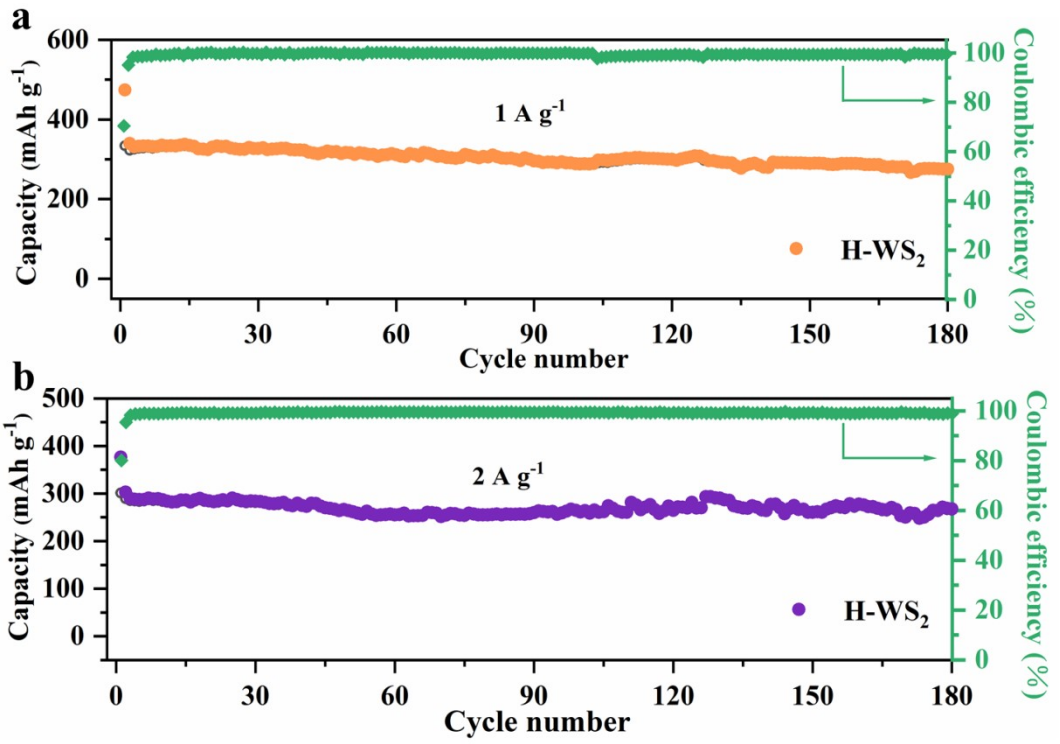

Fig. S11. Cycle performance of H-WS_2 electrodes at a current density of 1 A g^{-1} (a) and 2 A g^{-1} (b).

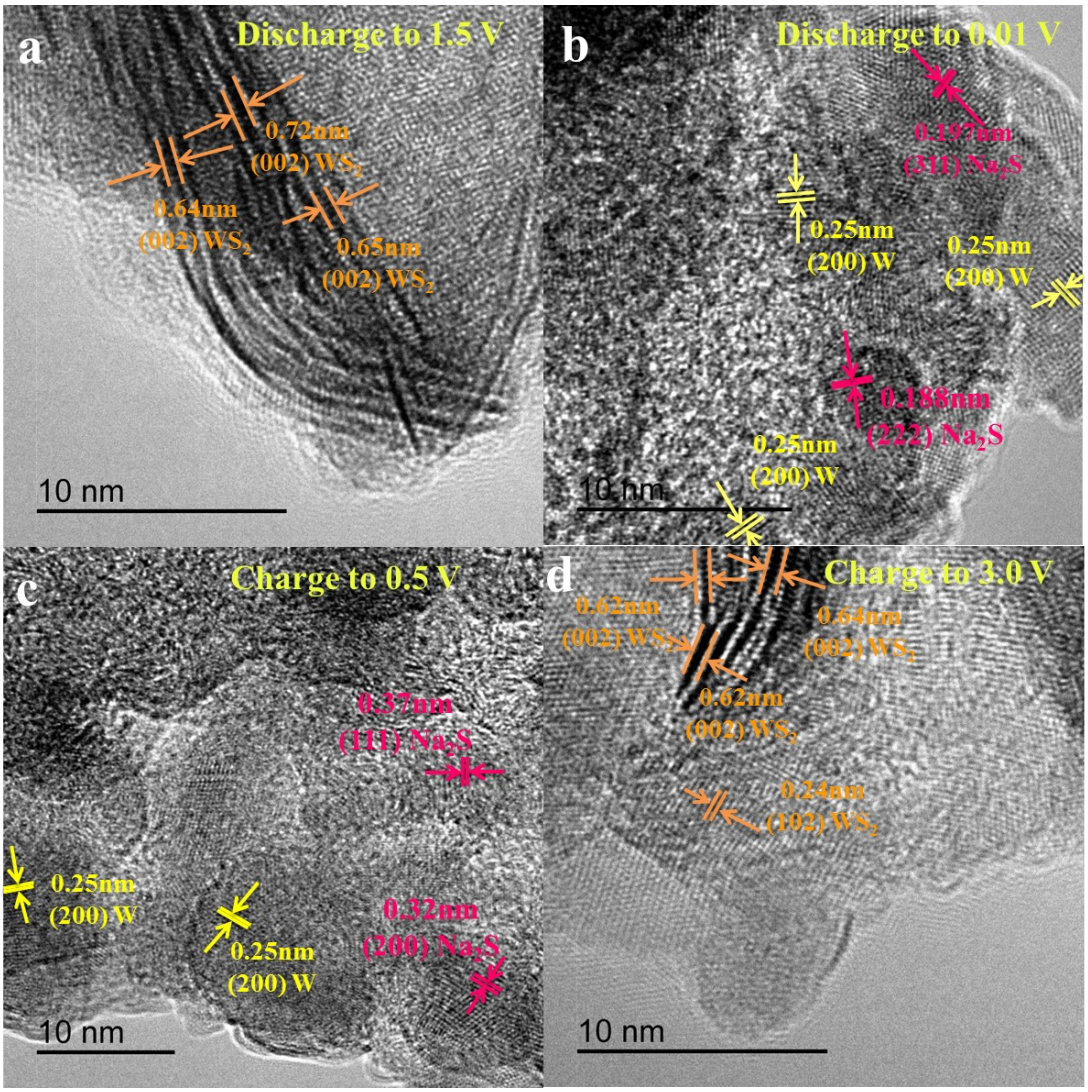

Fig. S12. *Ex-situ* transmission electron microscope images at different reaction stages in the first cycle of H-WS_2 electrode discharge to1.5 V (a) and 0.01 V (b); charge to 0.5 V(c) and 3 V (d).

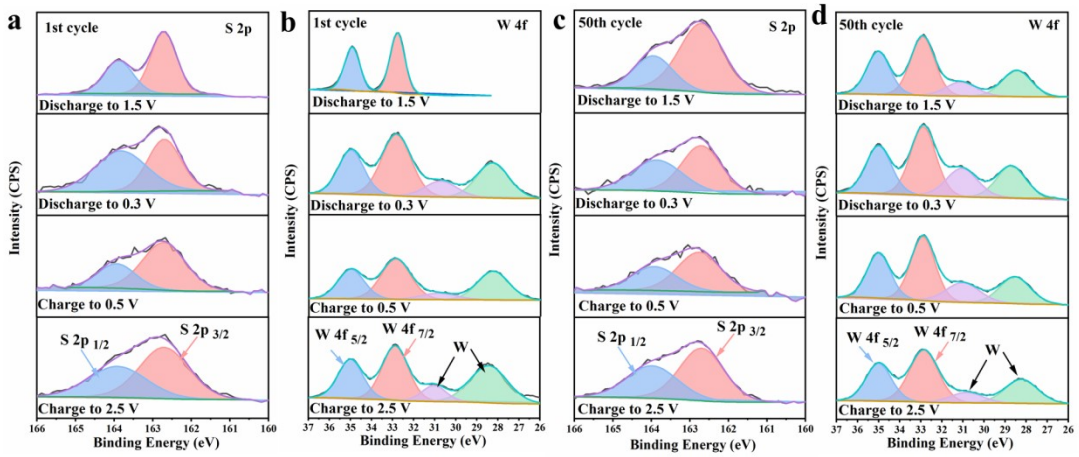

Fig. S13. Ex situ XPS analysis of H-WS_2 electrodes tested at various charge−discharge states for the 1st and 50th cycles.

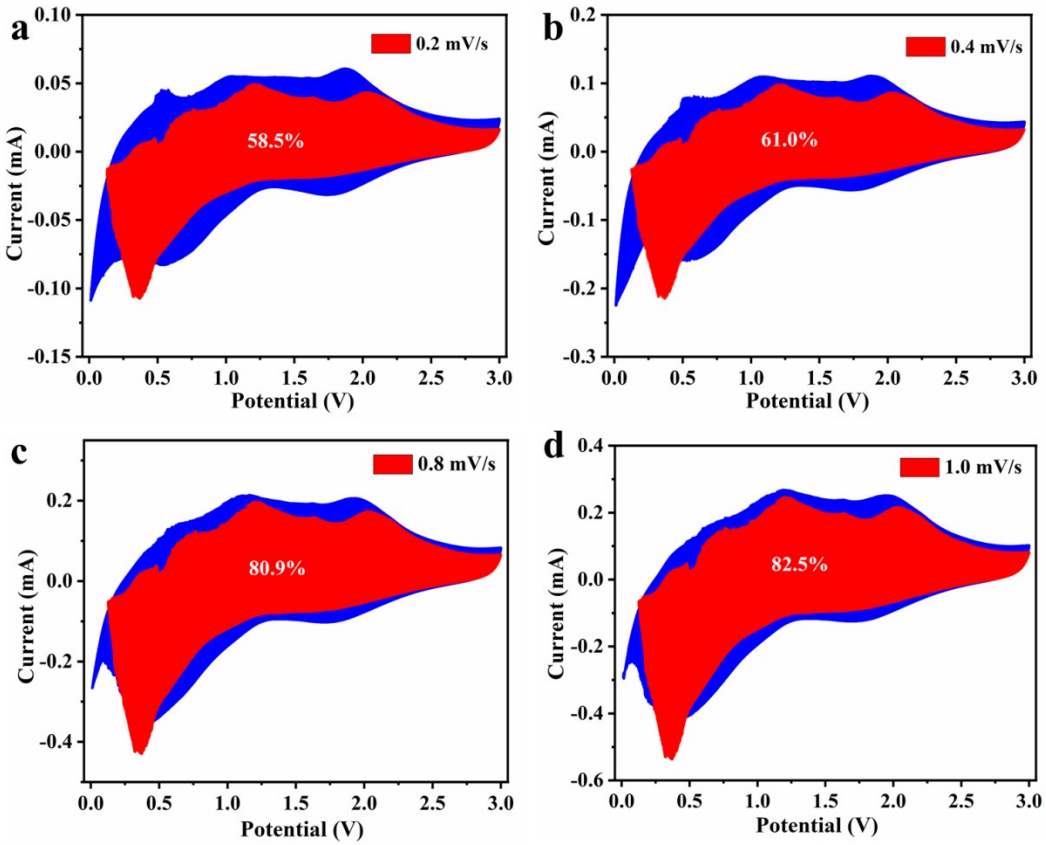

Fig. S14. Capacitive (red) and diffusion-controlled contribution to charge storage of H-WS_2 at (a) 0.2 mV s^{-1}; (b) 0.4 mV s^{-1}; (c) 0.8 mV s^{-1}; (d) 1.0 mV s^{-1}.

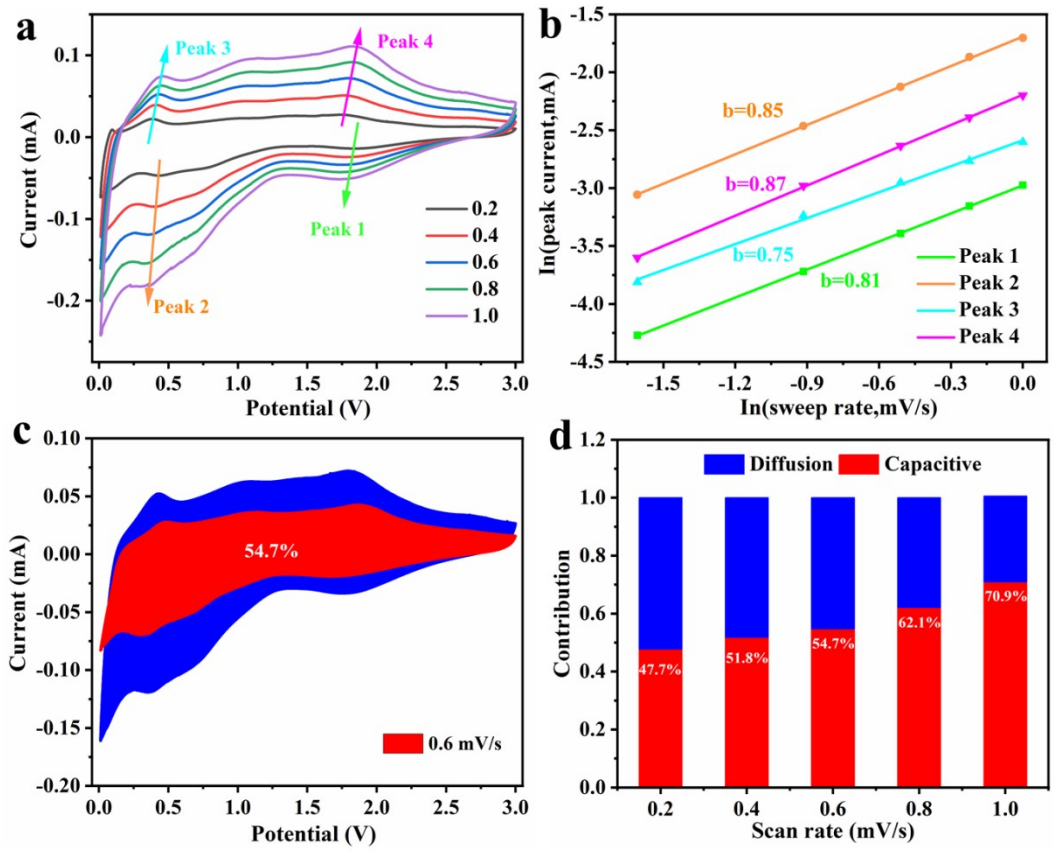

Fig. S15. Cyclic voltammograms of the electrodes at different scan rates for WS_2 (a); lni vs lnν plots of WS_2 (b); Capacitive (red) and diffusion-controlled contribution to charge storage of WS_2 (c) at 0.6 mV s^{-1}; normalized contribution ratios of capacitive (red) and diffusion-controlled capacities at different scan rates of WS_2 (d).

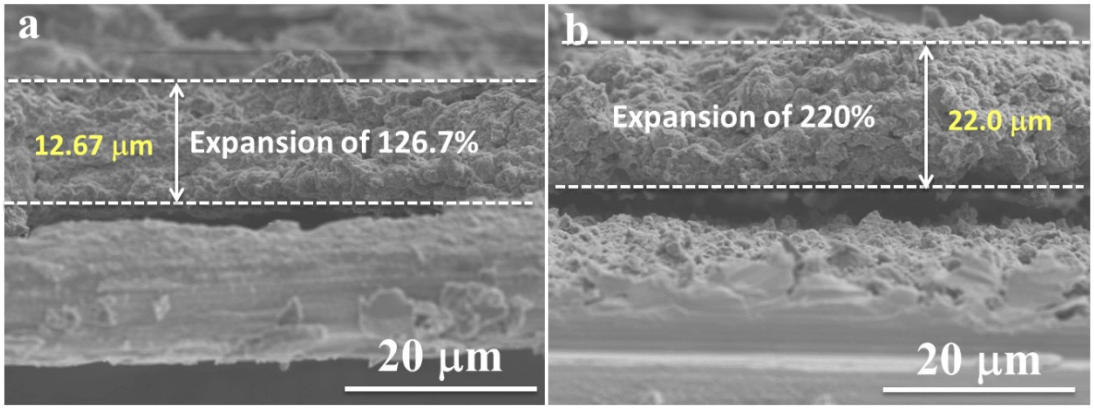

Fig. S16. The thickness of the H-WS_2 (a) and WS_2 (b) electrodes after 100 cycles.

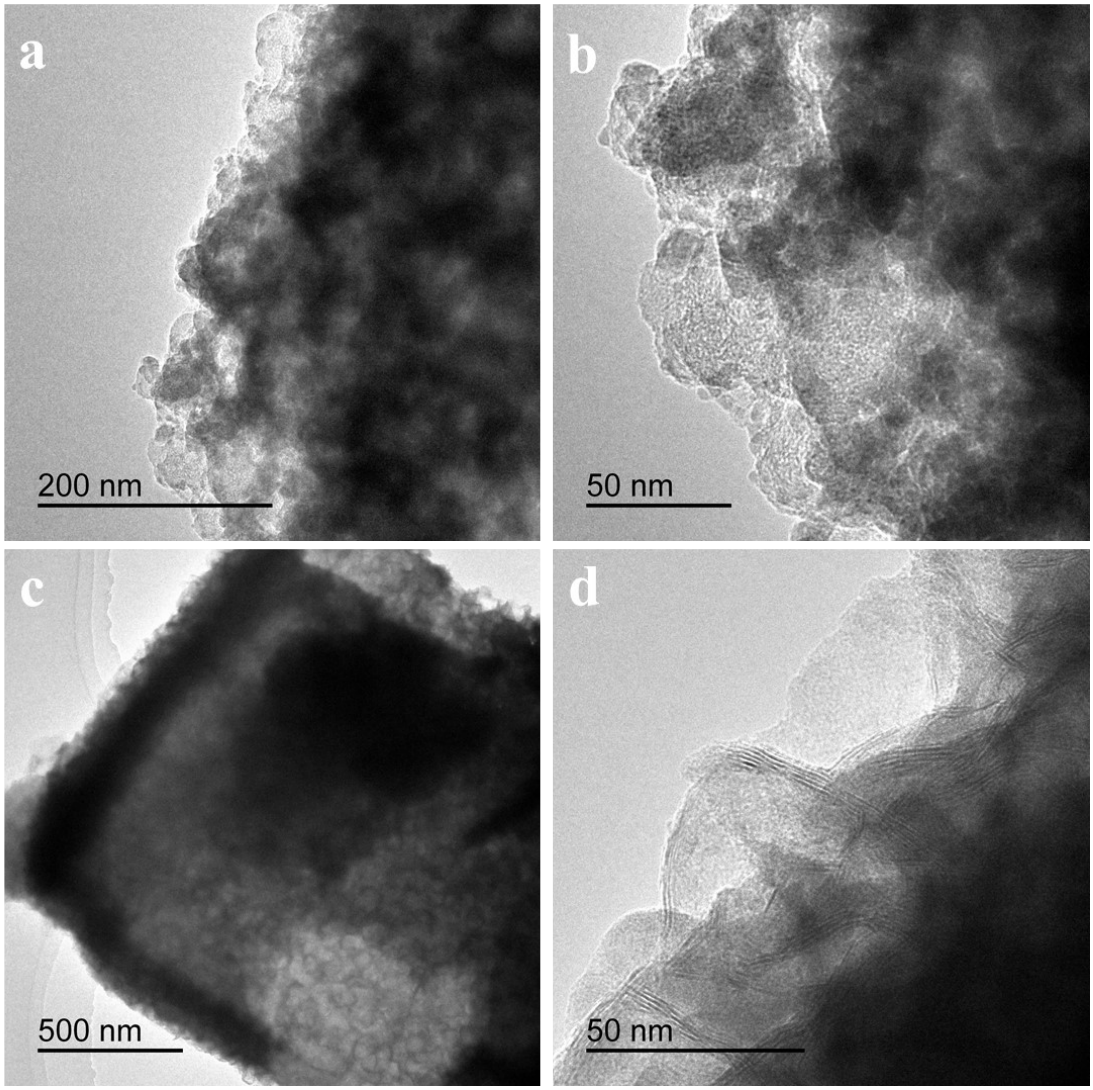

Fig. S17. Ex situ TEM images of WS_2 (a, b) and H-WS_2 (c, d) after 50 cycles.

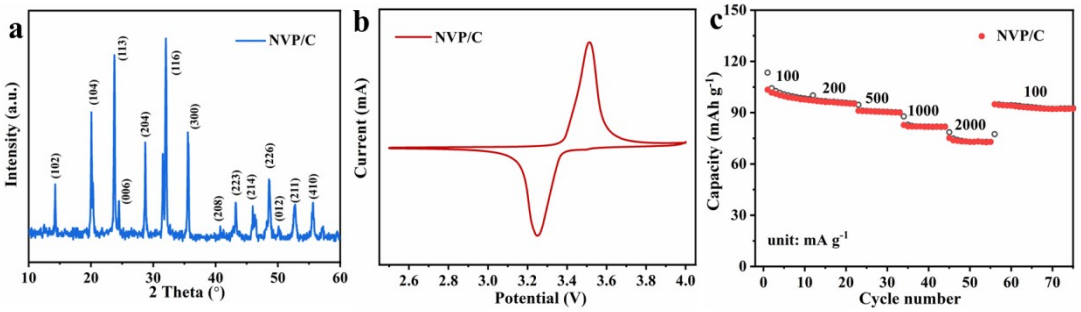

Fig. S18. (a) XRD patterns of $Na_3V_2(PO_4)_3$/C; (b) CV curve of $Na_3V_2(PO_4)_3$/C half cells at a scanning rate of 0.1 $mV \cdot s^{-1}$, the rate capacity of $Na_3V_2(PO_4)_3$/C half cells.